DOI: 10.1002/ejic.200900130

Parallel Crystallization of a "Static" and a Spin-Crossover Polymorph of an Iron(II) Complex from the Same Solution

Marco Haryono,[a] Frank W. Heinemann,[b] Konstantin Petukhov,[c] Klaus Gieb,[c] Paul Müller,[c] and Andreas Grohmann*[a]

Keywords: Iron / Spin crossover / Polymorphism / N ligands / Magnetic properties

The ligand 2,6-bis(1*H*-pyrazol-1-yl)-4-(thiocyanatomethyl)-pyridine (L) has been prepared from the hydroxymethyl precursor by OH/Br exchange and subsequent thiocyanate substitution. Two polymorphs of the unsolvated iron(II) complex $[Fe(L)_2](BF_4)_2$ crystallize at room temperature from the same solution (MeOH), and side by side. One (yellow) is high spin between 4 and 350 K, whereas the other (red-brown) shows spin crossover, with a thermal spin-transition centred at 272 K (width ca. 50 K). Both forms have been fully characterized by variable-temperature structure determination and magnetic susceptibility measurements. At a given temperature, the solid-state structures differ strongly with respect to the coordination geometry at iron(II), the orientation of the thiocyanatomethyl substituents, and cation-anion contacts. The implications of these structural differences for the observed spin behaviour are discussed.

Introduction

Spin crossover (SCO), or the reversible change of spin state in a transition metal complex in response to an external stimulus, is one of the oldest molecular switching phenomena known, and perhaps the most vital, considering its central role in haemoglobin-based respiration. The phenomenon, first described in the 1930s, has since been observed for many complexes, especially of iron (Fe^{II}, Fe^{III}) and cobalt, both in solution and in the crystalline state.[1–4] Spin-switchable iron(II) complexes (3 d^6), where the transition occurs between a state of maximum spin pairing (low spin, $^1A_{1g}/t_{2g}^6$) and maximum spin multiplicity (high spin, $^5T_{2g}/t_{2g}^4e_g^2$), are the most numerous, with the metal being found in a quasi-octahedral N_6 coordination environment in most cases. Ligand field strength and interelectronic interactions need to be carefully balanced, thus making the choice and combination of nitrogen ligands crucial, for the high- *and* the low-spin state to be accessible, depending on the external conditions. Stimuli known to induce spin crossover in suitably set up complexes include temperature, pressure, and light (*light-induced excited spin-state trapping*, or LIESST).[5] Even a subtle change in ligand field strength, as brought about by the photochemical switching of peripheral chromophores in an otherwise permanent coordination environment (*ligand-driven light-induced spin change*, or LD-LISC),[6] may cause a complex to alter its spin-state preference under a given set of external conditions. Packing effects in the solid-state structure which, depending on the type of counterion[7] or solvate/guest molecules,[8] may translate into different degrees of distortion of the coordination polyhedron, have similarly been identified as strong influences on the observed spin behaviour (it should be noted, however, that other effects, deriving from the change in chemical composition, cannot be excluded a priori).

The ls→hs transition entails the population of predominantly antibonding complex orbitals and is thus accompanied by a drastic change in geometric parameters (bond lengths, angles)[9,10] as the ionic radius of the metal increases and the complexes "swell". In the crystalline solid, these changes may be accompanied by a first-order phase transition; the proportion of complexes in the hs state, γ_{HS}, depends on the temperature but, at a given temperature, will also depend on the strength of interaction of coordination units within the lattice. The stronger these interactions, the steeper the graph $\gamma_{HS} = f(T)$ will be, and the greater the degree of steric and/or electronic cooperativity between the metal centres within the lattice. Thermally induced spin transitions, in particular, may show hysteresis, with the spin state depending on the history of the sample ("memory effect"). There are now a number of structurally well characterized compounds (mostly Fe^{II}) in the low- ($\gamma_{HS} = 0$) and high-spin states ($\gamma_{HS} = 1$), as well as mixtures ($0 \leq \gamma_{HS} \leq 1$) whose crystals contain both low-spin and high-spin (but otherwise identical) molecular entities.[11] Examples where a complex shows polymorphism as a consequence of different crystallization conditions, in other words different solid-

[a] Institut für Chemie, Technische Universität Berlin, Straße des 17. Juni 135, 10623 Berlin, Germany
Fax: +49-30-314-22935
E-mail: andreas.grohmann@chem.tu-berlin.de
[b] Department Chemie und Pharmazie, Universität Erlangen-Nürnberg, Egerlandstraße 1, 91058 Erlangen, Germany
[c] Department Physik, Universität Erlangen-Nürnberg, Erwin-Rommel-Straße 1, 91058 Erlangen, Germany

state structures with potentially different spin behaviour, are very rare.[12–14] Rarer still are cases where the molecular entity provides, in one crystallization experiment, materials of identical composition but with different spin behaviour, and we are aware of only a few previous examples.[15,16] The present report describes such a case, supported by temperature-dependent magnetochemical data, and outlines important structural differences between the polymorphs over a range of temperatures.

Results and Discussion

With a view to creating spin-switchable ensembles on surfaces, we are seeking to introduce suitable anchor groups into the organic backbone of iron complexes with known SCO behaviour.[17–19] The thiocyanato functionality (R-SCN) has recently been established as a viable precursor for thiolate monolayers on gold, giving $[Au(CN)_2]^-$ in the process.[20,21] Building upon work by Halcrow and co-workers,[22] and starting from the hydroxymethylene-substituted variant **1**[23] of 2,6-bis(pyrazol-1-yl)pyridine (Scheme 1), the introduction of a thiocyanate-bearing functionality in the *trans* position of the central pyridine ring to give **2** is straightforward.

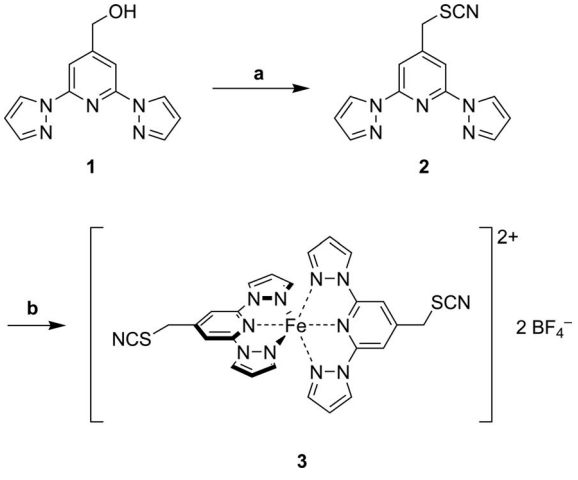

Scheme 1. a) PPh_3/Br_2, NH_4SCN, CH_3CN (75%); b) $Fe(BF_4)_2 \cdot 6H_2O$, thf (83%).

When thf solutions of $Fe(BF_4)_2 \cdot 6H_2O$ and **2** are mixed at room temperature (dinitrogen atmosphere), the desired homoleptic complex $[Fe(\mathbf{2})_2](BF_4)_2$ (**3**) is formed instantly as a yellow precipitate (83% yield). The elemental analysis data of this complex were in agreement with its proposed structure (see Exp. Section). We prepared single crystals of **3** for structural comparison with similar compounds,[24,25] and were intrigued to find that these preparations have different outcomes depending on the chosen conditions (Scheme 2).

Isothermal diffusion of diethyl ether into a methanol solution of **3** saturated at room temperature produces a uniform batch of yellow single crystals (**3a**; Scheme 2). The structure of the cation present in this type of crystal at 100 K is shown in Figure 1. The compound crystallizes in

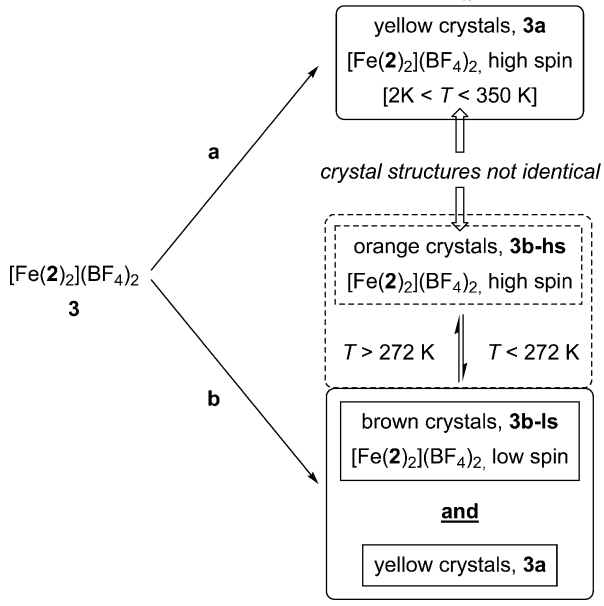

Scheme 2. Formation of polymorphs from **3**: a) crystallization from methanol solution saturated at room temperature; b) crystallization from methanol solution saturated at reflux.

the triclinic space group $P\bar{1}$ and has an asymmetric unit containing the complex cation and two BF_4^- counterions ($Z = 2$). The relative arrangement of the two tridentate ligands is skewed, which produces a strongly distorted iron coordination environment: the angle (ϕ) between the two iron–N(pyridine) bonds [N3–Fe1–N9 = 158.10(7)°] deviates considerably from the ideal value of 180°, and the interplanar angle θ (ideally 90°) is 78.84(2)°. The iron–nitrogen bond lengths are in the range 2.1264(18)–2.2430(19) Å, thus indicating high-spin iron(II). Parameters describing the conformation of the thiocyanatomethyl substituents are summarized in Table 1. The complex is paramagnetic between 2 and 350 K,[11] as shown by its magnetic susceptibility values over that range (Figure 2). $\chi_m T$ in the temperature range 40–150 K is between 3.05 and 3.18 $cm^3 mol^{-1} K$, in agreement with a quintet state (hs Fe^{II}).[26] After a small, reproducible increase

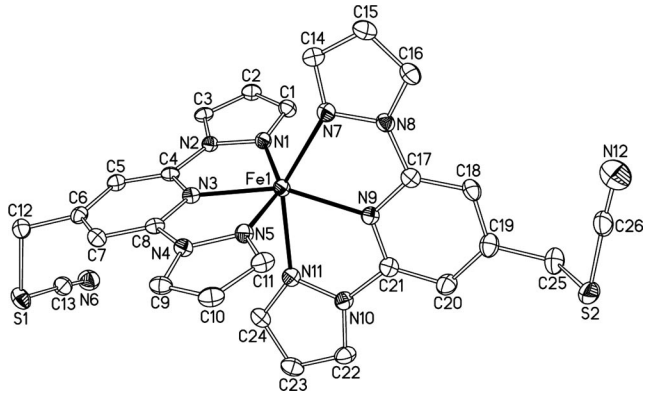

Figure 1. Structure of the $[Fe(\mathbf{2})_2]^{2+}$ dication in the crystal of **3a** (yellow) at 100 K (high spin). Hydrogen atoms have been omitted for clarity, and thermal ellipsoids are at the 50% probability level.

Table 1. Bond angles [°] and non-bonding distances [Å] involving the thiocyanatomethyl substituents in **3a** (hs, at 100 K and 313 K), **3b-ls** (100 K) and **3b-hs** (313 K).

Angle	**3a** (100 K)	**3a** (313 K)	**3b-ls** (100 K)	**3b-hs** (313 K)	Non-bonding distance	**3a** (100 K)	**3a** (313 K)	**3b-ls** (100 K)	**3b-hs** (313 K)
C6–C12–S1	111.1(2)	111.8(3)	108.1(1)	106.1(2)	C6···N6	3.950(4)	3.496(4)	4.836(2)	4.936(8)
C12–S1–C13	100.3(1)	109.3(6)	99.78(8)	99.6(2)					
C19–C25–S2	111.2(2)	111.6(4)	108.5(1)	107.0(2)	C19···N12	4.085(4)	4.050(4)	4.891(2)	4.986(8)
C25–S2–C26	98.7(2)	99.7(2)	100.03(8)	99.7(7)					

(0.37 $cm^3 mol^{-1} K$) between 150 and 180 K, $\chi_m T$ stays in the range 3.55–3.67 $cm^3 mol^{-1} K$ up to 350 K, which is still compatible with a quintet state. The temperature dependence, $\chi_m T/T$, is the same in both the warming and the cooling mode. The feature around 160 K may indicate a partial spin transition (of a small number of complex molecules in the crystal lattice).

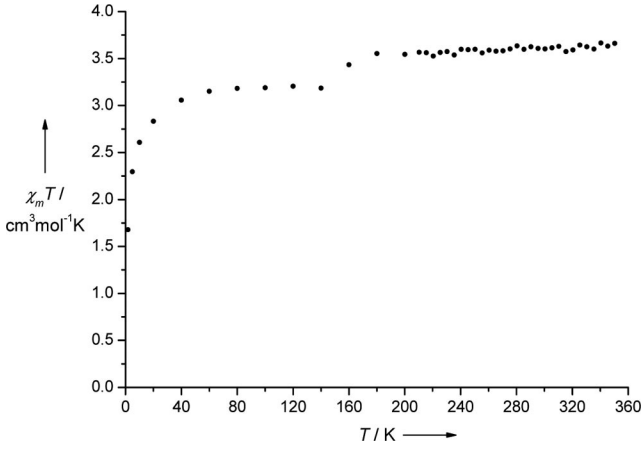

Figure 2. Magnetic susceptibility of **3a** (field strength: 0.1 T).

For the sake of comparison (see below), the structure of **3a** was also determined at 313 K, where the space group and composition of the unit cell remain unchanged. Both the thiocyanatomethyl groups and the tetrafluoroborate counterions are now considerably disordered, but the general geometry of the complex dication remains the same as at 100 K. The Fe–N bond lengths range from 2.125(2) to 2.233(2) Å, which denotes iron(II) in the high-spin state. The characteristic angles describing the geometry of the FeN_6 octahedron are θ = 81.94(2)° and ϕ = 161.76(8)°. The coordination octahedron is thus slightly less distorted at 313 K, as illustrated by the decrease of the parameters Σ and υ (Table 2). The main difference between the structures is the volume of the unit cell, which increases by 60.9(2) $Å^3$ to 1663.4(2) $Å^3$ at 313 K due to thermal expansion.

In a separate experiment, with the intention of optimizing the yield of single crystals, compound **3** was dissolved in methanol at reflux (60 °C) and the solution subsequently cooled to room temperature. Isothermal diffusion of ethyl ether into this solution now produced two readily distinguishable sorts of single crystals, yellow and reddish brown (see the graphical abstract for this paper), in an estimated proportion of 95:5. The X-ray diffraction data obtained for the yellow crystals reproduce structure **3a**. We initially surmised that the reddish brown fraction (**3b**) might be an oxidation product, or a product of methanolysis, although displacement of the strongly chelating bis(pyrazolyl)pyridine derivative appears unlikely, as does solvolysis of the SCN group, for which there is no reported precedent under the prevailing conditions. Alternatively, methanol is known to act as a reducing agent under certain conditions,[27] and we expected to clarify its role, if any, by structure analysis (cation/anion balance). The outcome of the preparation is reproducible. In subsequent crystallizations, we found that the fraction of reddish brown crystals (which grow at the gas-liquid interface) can be increased to approximately double its original amount by applying an excess pressure (approximately 0.8 atm) of dinitrogen to the crystallization vessel. It should be noted at this stage that, whereas elemental analysis of the red-brown crystals gave essentially the

Table 2. Temperature-dependent structural parameters of $[Fe(\mathbf{2})_2](BF_4)_2$ (**3**). The space group is $P\bar{1}$ at all temperatures. Parameters quantifying the distortion of the coordination polyhedron (ϕ, θ, Σ, υ) are based on the works of Elhaïk,[28] Mackovicky,[29] and Guionneau et al.[30]

	Spin state	T [K]	Mean Fe–N [Å]	Unit cell volume [$Å^3$]	α [°] [a]	ϕ [°] [b]	θ [°] [c]	Σ [°] [d]	υ [%] [e]
3b	low spin	100	1.95(4)	1579.4(3)	79.9(6)	178.22(6)	88.65	87.3	3.14
	low spin	150	1.95(4)	1587.5(2)	79.9(5)	178.22(6)	88.78	87.3	3.18
	low spin	200	1.95(4)	1599.6(2)	79.9(6)	178.19(7)	88.87	88.3	3.21
	high spin	278	2.11(4)	1646.0(2)	74.9(9)	174.00(8)	88.56	136.4	7.19
	high spin	313	2.15(4)	1661.0(3)	73.8(8)	172.34(8)	88.45	147.3	8.30
3a	high spin	100	2.17(4)	1602.4(2)	73.2(7)	158.10(7)	78.84	169.1	12.46
	high spin	313	2.17(4)	1663.4(2)	73.1(8)	161.76(8)	81.94	161.8	11.00

[a] Mean chelate bite angle $N_{pyridine}$–Fe–$N_{pyrazole}$. [b] Angle $N_{pyridine}$–Fe–$N_{pyridine}$. [c] Dihedral angle between the least-squares planes of the tridentate ligands. [d] $\Sigma = \sum_{i=1}^{12} |90 - \phi_i|$; ϕ: N–Fe–N angles between *cis*-positioned Fe–N bonds. [e] $\upsilon = 100[1 - \pi(V_P/V_s)]$; V_p: volume of the coordination polyhedron; V_s: volume of the circumscribed sphere (ideal octahedron: Σ = 0° and υ = 0%).

same data as for the yellow form, the IR spectra differ in the region diagnostic of the CN stretching vibration: the yellow polymorph has a single band at 2156 cm^{-1}, whereas this band is split (2149 and 2167 cm^{-1}) in the case of the red polymorph (see Exp. Section). X-ray data for **3b** were again collected at 100 K. The structure of the cation is shown in Figure 3.

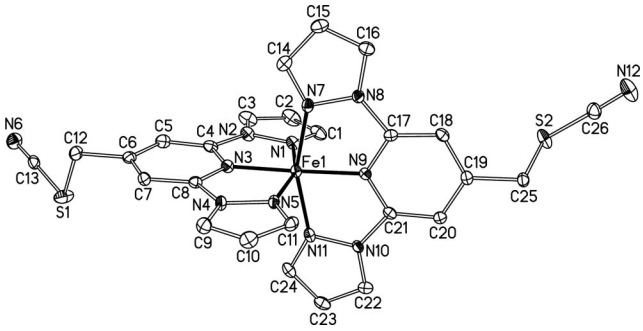

Figure 3. Structure of the $[Fe(\mathbf{2})_2]^{2+}$ dication in the crystal of **3b** (reddish brown) at 100 K (low spin). Hydrogen atoms have been omitted for clarity, and thermal ellipsoids are at the 50% probability level.

The space group is the same as for **3a** ($P\bar{1}$), and the asymmetric unit again contains the complex cation and two BF_4^- counterions ($Z = 2$), which means that the molecular compositions of **3a** and **3b** are identical. In the same way as **3a**, **3b** is unsolvated. The most striking difference in **3b** are the significantly shorter Fe–N bond lengths, which lie in the range 1.8966(13)–1.9862(14) Å, thereby suggesting low-spin iron(II). The (*mer*-NNN)$_2$ donor set has close to ideal D_{2d} symmetry: the angle N3–Fe1–N9 is 178.22(6)°, and the best planes of the ligands are virtually orthogonal at 88.65(0)°. SQUID magnetometry of **3b** (between 5 and 350 K, Figure 4) reveals an entirely different behaviour from **3a**: the graph shows a thermal transition centred at 272 K from the high-spin ($\chi_m T$ in the range 3.28–3.61 $cm^3 mol^{-1} K$) to the low-spin state ($\chi_m T \leq 0.3\ cm^3 mol^{-1} K$), with a width of around 50 K. The process is reversible with a hysteresis so small (<2 K) as to be insignificant. The crystals are thermochromic, showing a dark brown colour at liquid nitrogen temperature and an orange colour when heated to 350 K.

In order to monitor a possible temperature-dependent interconversion of **3a** and **3b**, we chose a single crystal of the latter and collected its diffraction data at four additional temperatures (150, 200, 278, and 313 K, in this order), below and above its spin-transition temperature ($T_{1/2}$) of 272 K. All structures are in the same space group ($P\bar{1}$). The two structures determined below $T_{1/2}$ have parameters similar to the structure measured at 100 K. Similar to the minor variation of cell constants, which reflects the thermal expansion of the crystal, there is only an insignificant change in Fe–N bond lengths (the average being 1.95 Å throughout), thus indicating a low-spin configuration for iron(II) at 150 and 200 K also (Table 2).

The structures determined at 278 and 313 K are very similar to each other, but markedly different from the three

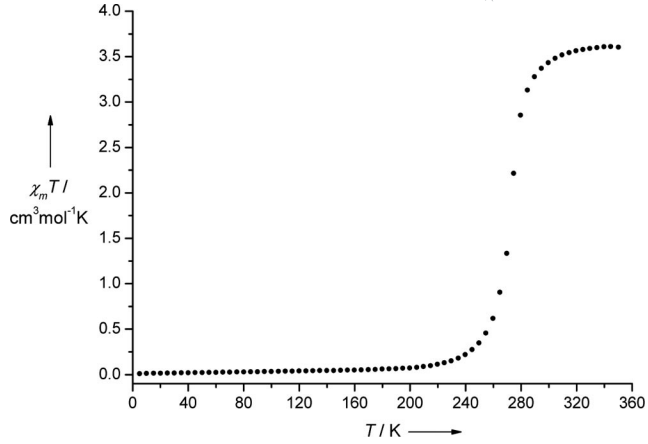

Figure 4. Magnetic susceptibility of **3b** (field strength: 0.1 T).

low-temperature structures (Figure 5 shows the cation structure at 313 K). Thus, the mean Fe–N bond lengths are 2.11 and 2.15 Å, respectively, an increase of around 10% over the low-temperature structures (0.16–0.20 Å in absolute terms) and typical for high-spin iron(II).[3,10] Overall, the respective coordination polyhedra show different degrees of distortion, which may be conveniently quantified in terms of the parameters Σ and υ as defined in Table 2.[29,30] Both parameters increase considerably for the hs structures, thereby reflecting an increasing deviation from near D_{2d} symmetry, in keeping with data reported by Halcrow et al.[25,28] A plot of unit cell volume vs. temperature (Figure 6) shows a change in gradient at around $T_{1/2}$, as expected for a thermal spin transition.

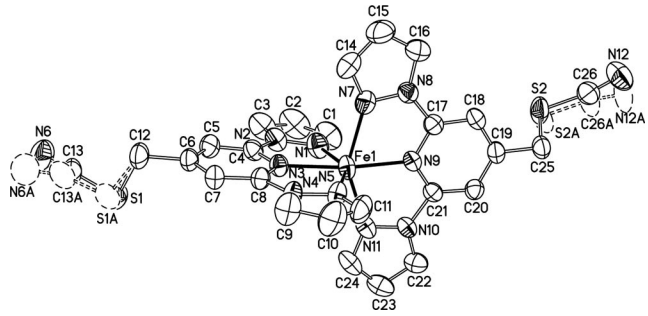

Figure 5. Structure of the $[Fe(\mathbf{2})_2]^{2+}$ dication in the crystal of **3b** at 313 K (high spin, **3b-hs**). Hydrogen atoms have been omitted for clarity, and thermal ellipsoids are at the 50% probability level.

Whereas **3a** is high spin over the whole temperature range in the solid state, **3b** shows typical spin-crossover behaviour over the same range, in agreement with Halcrow's analysis of coordination geometry vs. spin behaviour in related complexes.[11] Remarkably, the two high-spin structures, (**3a** and **3b-hs**; cf. Figures 1 and 5) are *not the same*, as can readily be seen from the parameters listed in Tables 1 and 2. Specifically, the conformations of the thiocyanatomethyl substituents differ strongly, as indicated by the nonbonded C6···N6 and C19···N12 distances (Table 1). It seems likely that the different orientations of these groups, in a manner similar to the LD-LISC phenomenon referred to in the Introduction, attenuate the ligand field and thus have a

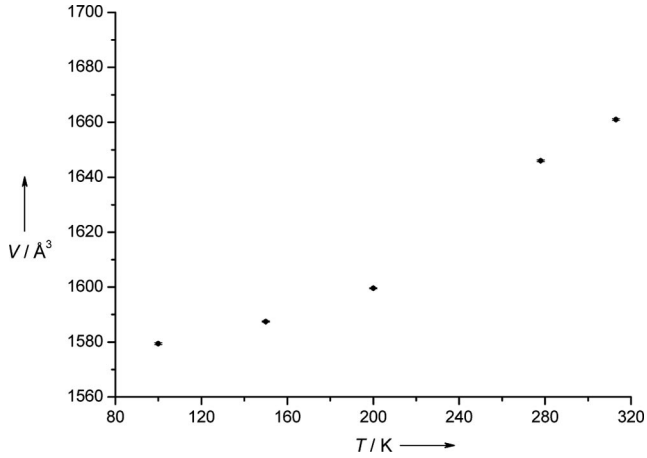

Figure 6. Plot of unit cell volume of **3b** as a function of temperature.

direct influence on the coordination geometry, and hence spin behaviour, in the solid state. The crystalline form **3a** loses its temperature-independent high-spin character in solution (acetonitrile), which shows thermal spin-crossover in the temperature range 194–293 K, as shown in Figure 7 (^{1}H NMR spectroscopy, Evans method).[31,32] At 293 K, $\chi_m T$ is 3.1(1) $cm^3 mol^{-1} K$, thus indicating high-spin iron(II). $\chi_m T$ decreases gradually on cooling, reaching a value of 1.1(1) $cm^3 mol^{-1} K$ at 194 K, the lowest temperature accessible in CD_3CN.

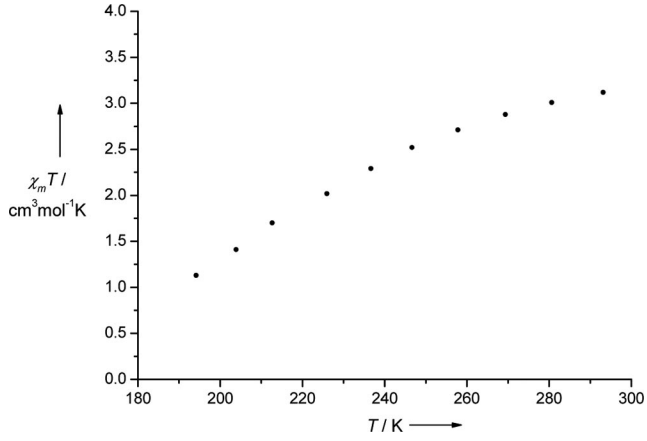

Figure 7. Plot of $\chi_m T$ vs. T for **3a** in CD_3CN (Evans method).

As has also been mentioned in the Introduction, the spin-transition characteristics of an SCO compound in the solid state are not defined only at the molecular level (coordination geometry)[14] but also *inter*molecularly, as SCO-related bond-length changes amount to a transmission of information between molecular entities in the crystal lattice. The extended solid-state structures of the two high-spin forms (**3a** and **3b-hs**) differ in their cation-anion arrangement, as shown in Figure 8. Thus, crystals of **3a** contain alternating cation and anion layers (BF_4^-) whereas crystals of **3b-hs** (unit cell represented in an orientation similar to **3a**) have their cations and anions more uniformly distributed. Most importantly, perhaps, there are S···F–B contacts [d(S1···F14) = 3.017(5) Å, shorter than the sum of the van der Waals radii of S and F] in the structure of **3b-hs**, but no such contacts in the structure of **3a**.[33] These contacts likely cause the splitting of the ν(CN) absorption band in the IR spectrum of **3b**, a phenomenon not observed in the spectrum of **3a**. All other intermolecular distances are unexceptional in both structures. Whereas the observations made by Reger et al.[16] suggest that, when comparing polymorphs, the more "loosely" organized structure (in the sense that there are fewer secondary interactions in all three directions of space) is more prone to show spin crossover, our findings do not immediately lend themselves to this interpretation. Furthermore, neither structure shows the "terpyridine embrace" motif that has recently been reviewed for complexes containing the structural element $[M(terpy)_2]^{2+}$.[34]

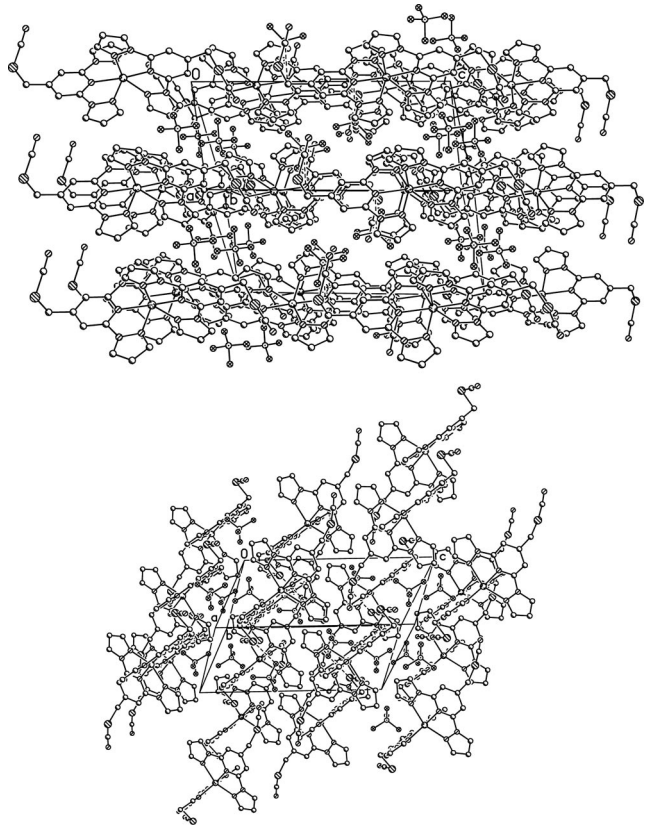

Figure 8. Comparison of the supramolecular structures of the high-spin forms **3a** (top) and **3b-hs** (bottom); unit cell origin at top left, *c*-axis to the right in both cases. Cation and anion layers (BF_4^-) alternate in the crystals of **3a**, whereas crystals of **3b-hs** (unit cell represented in an orientation similar to **3a**) have their cations and anions more uniformly distributed (see text).

Conclusions

The $Fe^{II}N_6$ coordination compound presented in this study, namely $[Fe(\mathbf{2})_2](BF_4)_2$ (**3**), is a rare example where polymorphs with different spin characteristics are accessible simultaneously from the same crystallization reaction. This compound is an interesting candidate for theoretical analy-

sis as it allows us to study the influence of changes in the molecular structure (conformation of the peripheral thiocyanatomethyl groups) on the ligand field strength, as well as the influence of these changes on the 3D lattice structure, and vice versa, in the absence of counterion or solvate effects. The underlying cause for the coordination chemical flexibility manifest in compound **3** is an angular Jahn–Teller distortion at the iron centre.[11] On a historical note, compound **3** presents a case of spin-state isomerism (**3a** vs. **3b-ls**),[35,36] and at the same time is a true example of distortional isomerism (**3a** vs. **3b-hs**), the latter being related to "bond-stretch isomerism" which, at least in the context of coordination chemistry, is a contentious concept of some historical notoriety.[37] Our findings underscore the interdependence of molecular and supramolecular effects in spin-transition materials, and at the same time highlight the potential pitfalls inherent in the "programming" of SCO behaviour into bulk phases, both in three dimensions and, in the future, in two.

Experimental Section

Materials and Instrumentation: Unless noted otherwise, all reactions were carried out in dry solvents under dry dinitrogen, using standard Schlenk techniques. Compound **1** was synthesized according to a literature procedure.[23] All other chemicals were purchased from Aldrich and used without further purification. IR spectra were measured as KBr disks. Spectroscopic data were obtained using the following instruments: IR spectroscopy: Nicolet Magna System 750; NMR spectroscopy: Bruker ARX 200 and ARX 400. Elemental analyses were carried out using a Thermo Finnigan, Flash EA, 1112 series analyzer. Solid-state variable-temperature magnetic susceptibility measurements were performed using a Quantum Design MPMS-XL5 SQUID (superconducting quantum interference device) magnetometer operating at 0.1 T. Diamagnetic corrections for the sample and the sample holder were applied. Magnetic susceptibility measurements in solution (CD_3CN/TMS = 99:1 v/v) were obtained by the Evans method[31,32] using a Bruker ARX 400 spectrometer operating at 400 MHz.

2,6-Bis(1*H*-pyrazol-1-yl)-4-(thiocyanatomethyl)pyridine (2): A solution of bromine (0.11 mL, 2.2 mmol) in acetonitrile (1.1 mL) was added dropwise at room temperature to a solution of PPh_3 (570 mg, 2.2 mmol) in acetonitrile (5.5 mL). A solution of NH_4SCN (329 mg, 4.3 mmol) in acetonitrile (7.4 mL) was then added. A solution of compound **1** (500 mg, 2.1 mmol) in acetonitrile (9 mL) was finally added, and the mixture stirred at room temperature for 24 h. The resulting suspension was filtered, and the solid washed with acetonitrile. The filtrate was collected, the solvent removed on a rotary evaporator and the residue purified by column chromatography on silica gel using hexane/ethyl acetate (1:1) as eluent (R_f = 0.59) to give thiocyanate **2** as a white solid (440 mg, 75%). ^{1}H NMR (200 MHz, [D]chloroform, 25 °C): δ = 8.57 (dd, J = 2.7, 0.6 Hz, 2 H; CH=N), 7.90 (s, 2 H, py-H), 7.79 (dd, J = 1.6, 0.6 Hz, 2 H; CH=N), 6.53 (dd, J = 2.7, 1.7 Hz, 2 H; CH=C), 4.21 (s, 2 H, CH_2) ppm. ^{13}C NMR (100.6 MHz, [D]-chloroform, 25 °C): δ = 150.6 (py-$C^{2,6}$), 149.0 (py-C^4), 142.7 (N=CH), 127.2 (N-CH), 110.6 (SCN), 109.0 (py-$C^{3,5}$), 108.3 (CH), 36.6 (CH_2) ppm. IR (KBr): $\tilde{\nu}$ = 618 (m), 705 (m), 779 (s), 954 (s), 1043 (s), 1207 (s), 1396 (br), 1465 (br), 1520 (s), 1573 (s), 1620 (s), 2160 (s), 3134 (m). $C_{13}H_{10}N_6S$ (282.32): calcd. C 55.30, H 3.57, N 29.77, S 11.36; found C 55.37, H 3.61, N 29.99, S 11.60.

[Fe(2)$_2$](BF$_4$)$_2$ (3): A solution of $Fe(BF_4)_2 \cdot 6H_2O$ (87 mg, 0.3 mmol) in thf (3 mL) was added to a solution of compound **2** (150 mg, 0.5 mmol) in thf (5 mL). A yellow solid immediately precipitated from the solution, and the mixture was stirred for 18 h at room temperature. The precipitate was filtered, washed with thf and dried in vacuo to yield complex **3** as a yellow powder (172 mg, 83%). Single crystals of compound **3** were prepared by two different methods.

Method A: Isothermal diffusion of diethyl ether at room temperature into a solution of **3** in methanol, saturated at room temperature, yielded yellow crystals.

Method B: Isothermal diffusion of diethyl ether at room temperature into a solution of **3** in methanol (c = 15 mg/l), saturated at reflux temperature, under an excess pressure of N_2 (0.8 atm) in a pressure-resistant glass vessel, yielded a mixture of yellow (**3a**) and reddish brown (**3b**) crystals after one week. ^{1}H NMR (200 MHz, [D_3]acetonitrile, 25 °C): δ = 66.48 (s), 58.77 (s), 39.26 (s), 37.97 (s), 4.86 (s) (all signals are paramagnetically broadened) ppm. **3a**: IR (KBr): $\tilde{\nu}$ = 521 (w), 597 (w), 704 (w), 769 (m), 793 (m), 861 (w), 917 (w), 971 (s), 1052 (vs), 1089 (vs), 1176 (w), 1215 (w), 1249 (w), 1287 (m), 1311 (m), 1337 (m), 1406 (s), 1467 (vs), 1527 (s), 1581 (m), 1630 (s), 2156 (m), 3136 (m). $C_{26}H_{20}B_2F_8FeN_{12}S_2$ (794.10): calcd. C 39.32, H 2.54, N 21.17, S 8.08; found C 39.62, H 2.60, N 20.62, S 7.90. **3b**: IR (KBr): $\tilde{\nu}$ = 520 (m), 598 (m), 617 (m), 765 (s), 793 (m), 860 (m), 912 (m), 972 (s), 1050 (vs), 1089 (vs), 1177 (m), 1214 (m), 1222 (m), 1244 (w), 1287 (m), 1312 (m), 1338 (s), 1405 (vs), 1467 (vs), 1527 (s), 1582 (s), 1631 (s), 2149 (m), 2167 (m), 3126 (m). $C_{26}H_{20}B_2F_8FeN_{12}S_2$ (794.10): calcd. C 39.32, H 2.54, N 21.17, S 8.08; found C 39.66, H 2.44, N 20.82, S 7.82.

X-ray Crystallography: Crystal data and details concerning data collection and refinement are given in Table 3. Data collection was performed with a Bruker-Nonius KappaCCD diffractometer using graphite-monochromated Mo-K_α radiation (λ = 0.71073 Å). The COLLECT suite[38] was used for data collection and integration. All structures were solved by direct methods and refined by full-matrix least-squares procedures on F^2 using the program SHELXTL NT 6.12.[39] All non-hydrogen atoms were refined anisotropically. Disorder: **3a_100K**: one MeSCN group (atoms S2, C25, C26), two preferential orientations refined [occupation 87.5(2):12.5(2)%]; one BF_4^- ion (atoms F22–F24), two preferential orientations refined [occupation 74.9(4):25.1(4)%]; **3a_313K**: both MeSCN groups (atoms S1, C13, N6 and C25, S2, C26), two preferential orientations refined [occupation 58.6(8):41.4(8)% and 79.2(3):20.8(3)%]; both BF_4^- ions (atoms B1–F14 and F22–F24), two preferential orientations refined [occupation 52.3(8):47.7(8)% and 57.6(8):42.4(8)%]; **3b_200K**: one MeSCN group (atoms S2, C26, N12), two preferential orientations refined [occupation 78(3):22(3)%]; **3b_278K**: both MeSCN groups (atoms S1, C13, N6 and S2, C26, N12), two preferential orientations refined [occupation 86.4(8):13.6(8)% and 64(4):36(4)%]; one BF_4^- ion (atoms F21–F24), two preferential orientations refined [occupation 77(2):23(2)%]; **3b_313K**: both MeSCN groups (atoms S1, C13, N6 and S2, C26, N12), two preferential orientations refined [occupation 80(1):20(1)% and 62(4):38(4)%]; both BF_4^- ions (atoms F11–F14 and F21–F24), two preferential orientations refined [occupation 86.4(4):13.6(4)% and 74(2):26(2)%]. The hydrogen atoms were placed in positions of optimized geometry, and their isotropic displacement parameters were tied to those of the corresponding carrier atoms by a factor of 1.2. The geometrical features of the structures were analyzed using the programs IVTON[40] and MERCURY v1.4.2.[41]

CCDC-699523 (for **3a_100K**), -699524 (for **3a_313K**), -699525 (for **3b_100K**), -699526 (for **3b_150K**), -699527 (for **3b_200K**), -699528

Table 3. Crystal data for the polymorphs of $[Fe(\mathbf{2})_2](BF_4)_2$. The space group is $P\bar{1}$ (triclinic), $Z = 2$, and the molecular composition is $C_{26}H_{20}B_2F_8FeN_{12}S_2$ in all cases.

	3a_100K	**3a_313K**	**3b_100K**	**3b_150K**	**3b_200K**	**3b_278K**	**3b_313K**
T [K]	100	313	100	150	200	278	313
Spin state	high spin	high spin	low spin	low spin	low spin	high spin	high spin
Crystal size [mm]	0.23×0.23×0.14	0.42×0.26×0.12	0.25×0.18×0.12	0.41×0.28×0.18	0.41×0.28×0.18	0.41×0.28×0.18	0.41×0.28×0.18
colour	yellow	yellow	brown	brown	brown	red-brown	orange
a [Å]	8.0542(5)	8.2151(4)	8.4185(8)	8.4395(6)	8.4624(8)	8.4848(7)	8.4976(9)
b [Å]	12.1047(7)	12.3119(9)	13.4168(7)	13.4235(4)	13.4479(6)	13.5074(6)	13.5192(14)
c [Å]	17.3154(13)	17.3277(11)	15.577(2)	15.6000(13)	15.6397(9)	16.0828(16)	16.2194(14)
α [°]	87.080(5)	87.784(6)	98.231(7)	98.238(4)	98.301(6)	99.246(6)	99.583(5)
β [°]	78.111(6)	79.607(5)	104.417(9)	104.392(6)	104.293(6)	105.059(8)	105.071(8)
γ [°]	75.938(5)	74.788(5)	107.479(5)	107.409(3)	107.374(5)	106.943(4)	106.932(4)
V [Å^3]	1602.43(18)	1663.36(18)	1579.4(3)	1587.5(2)	1599.6(2)	1646.0(3)	1661.0(3)
$\rho_{calcd.}$ [g cm^{-3}]	1.646	1.586	1.670	1.661	1.649	1.602	1.588
μ [mm^{-1}]	0.690	0.664	0.700	0.696	0.691	0.671	0.665
Absorption correction	SADABS[a]	SADABS	SADABS	SADABS	SADABS	SADABS	SADABS
T_{min}/T_{max}	0.849/0.908	0.770/0.910	0.799/0.919	0.708/0.880	0.708/0.880	0.708/0.880	0.708/0.880
Scan	ϕ- and ω-rotations with 2.0° and 140 s per frame	ϕ- and ω-rotations with 2.0° and 100 s per frame	ϕ- and ω-rotations with 2.0° and 116 s per frame	ϕ- and ω-rotations with 2.0° and 100 s per frame	ϕ- and ω-rotations with 2.0° and 56 s per frame	ϕ- and ω-rotations with 2.0° and 120 s per frame	ϕ- and ω-rotations with 2.0° and 120 s per frame
2θ range [°]	6.2–54.2	5.8–54.2	6.2–55.8	6.2–55.0	6.2–55.0	6.2–55.0	6.2–55.0
Measured reflections	29030	57716	38352	37716	33721	38758	37755
Unique reflections	7034	7313	7521	7276	7328	7496	7582
Observed reflections[b]	5450	5627	6183	6286	5906	5604	5312
Refined parameters	516	590	460	460	488	553	590
wR_2 (all data) [c]	0.0907	0.1364	0.0670	0.0677	0.0762	0.1222	0.1200
$R1$ (observed data) [d]	0.0385	0.0484	0.0301	0.0284	0.0326	0.0471	0.0456
ρ_{fin} (max./min.) [e Å^{-3}]	0.593/–0.406	0.491/–0.391	0.401/–0.442	0.590/–0.646	0.785/–0.690	0.485/–0.370	0.480/–0.347
Weighting scheme[e]	$k = 0.0343$/ $l = 1.5946$	$k = 0.0645$/ $l = 1.1903$	$k = 0.0224$/ $l = 1.2814$	$k = 0.0230$/ $l = 1.3274$	$k = 0.0256$/ $l = 1.2332$	$k = 0.0507$/ $l = 1.2830$	$k = 0.0230$/ $l = 1.3274$

[a] *SADABS 2.06*, Bruker AXS Inc., **2002**, Madison WI, U.S.A. [b] With $F_o \geq 4\sigma(F)$. [c] $wR_2 = [\Sigma[w(F_o^2 - F_c^2)^2]/\Sigma[w(F_o^2)^2]]^{1/2}$. [d] $R1 = \Sigma||F_o| - |F_c||/\Sigma|F_o|$ for $F_o \geq 4\sigma(F)$. [e] $w = 1/[\sigma^2(F_o^2) + (kP)^2 + lP]$ and $P = (F_o^2) + 2F_c^2)/3$.

(for **3b_278K**), and -699529 (for **3b_313K**) contain the supplementary crystallographic data. These data can be obtained free of charge from the Cambridge Crystallographic Data Centre via www.ccdc.cam.ac.uk/data_request/cif.

Acknowledgments

Support of this work by the Deutsche Forschungsgemeinschaft (DFG) (Sonderforschungsbereich 658, Elementary Processes in Molecular Switches on Surfaces) is gratefully acknowledged.

[1] P. Gütlich, Y. Garcia, H. A. Goodwin, *Chem. Soc. Rev.* **2000**, *29*, 419–427.
[2] P. Gütlich, H. A. Goodwin, *Top. Curr. Chem.* **2004**, 233–235.
[3] P. Gütlich, A. Hauser, H. Spiering, *Angew. Chem. Int. Ed. Engl.* **1994**, *33*, 2024–2054.
[4] J. A. Real, A. B. Gaspar, M. C. Muñoz, *Dalton Trans.* **2005**, 2062–2079.
[5] P. Gütlich, Y. Garcia, T. Woike, *Coord. Chem. Rev.* **2001**, *219–221*, 839–879.
[6] M.-L. Boillot, J. Zarembowitch, A. Sour, *Top. Curr. Chem.* **2004**, *234*, 261–276.
[7] C. Carbonera, C. A. Kilner, J.-F. Letard, M. A. Halcrow, *Dalton Trans.* **2007**, 1284–1292.
[8] M. Hostettler, K. W. Törnroos, D. Chernyshov, B. Vangdal, H.-B. Bürgi, *Angew. Chem. Int. Ed.* **2004**, *43*, 4589–4594.
[9] A. Hauser, J. Jeftic, H. Romstedt, R. Hinek, H. Spiering, *Coord. Chem. Rev.* **1999**, *190–192*, 471–491.
[10] E. König, *Struct. Bonding (Berlin)* **1991**, *76*, 51–152.
[11] J. Elhaïk, C. A. Kilner, M. A. Halcrow, *Dalton Trans.* **2006**, 823–830.
[12] A. Ozarowski, B. R. McGarvey, A. B. Sarkar, J. E. Drake, *Inorg. Chem.* **1988**, *27*, 628–635.
[13] C. Rajadurai, Z. Qu, O. Fuhr, B. Gopalan, R. Kruk, M. Ghafari, M. Ruben, *Dalton Trans.* **2007**, 3531–3537.
[14] S. Zein, G. S. Matouzenko, S. A. Borshch, *J. Phys. Chem. A* **2005**, *109*, 8568–8571.
[15] G. Matouzenko, A. Bousseksou, S. Lecoq, P. J. van Koningsbruggen, M. Perrin, O. Kahn, A. Collet, *Inorg. Chem.* **1997**, *36*, 5869–5879.
[16] D. L. Reger, J. R. Gardinier, M. D. Smith, A. M. Shahin, G. J. Long, L. Rebbouh, F. Grandjean, *Inorg. Chem.* **2005**, *44*, 1852–1866.
[17] M. A. Halcrow, *Polyhedron* **2007**, *26*, 3523–3576.
[18] J. Pitarch López, H. Kämpf, M. Grunert, P. Gütlich, F. W. Heinemann, R. Prakash, A. Grohmann, *Chem. Commun.* **2006**, 1718–1720.
[19] a) C. Shen, M. Haryono, A. Grohmann, M. Buck, T. Weidner, N. Ballav, M. Zharnikov, *Langmuir* **2008**, *24*, 12883–12891; b) R. Chandrasekar, F. Schramm, O. Fuhr, M. Ruben, *Eur. J. Inorg. Chem.* **2008**, 2649.
[20] J. W. Ciszek, J. M. Tour, *Chem. Mater.* **2005**, *17*, 5684–5690.
[21] C. Shen, M. Buck, J. D. E. T. Wilton-Ely, T. Weidner, M. Zharnikov, *Langmuir* **2008**, *24*, 6609–6615.
[22] M. A. Halcrow, *Coord. Chem. Rev.* **2005**, *249*, 2880–2908.
[23] J. Elhaïk, C. M. Pask, C. A. Kilner, M. A. Halcrow, *Tetrahedron* **2007**, *63*, 291–298.
[24] J. M. Holland, J. A. McAllister, C. A. Kilner, M. Thornton-Pett, A. J. Bridgeman, M. A. Halcrow, *J. Chem. Soc., Dalton Trans.* **2002**, 548–554.
[25] V. A. Money, J. Elhaik, M. A. Halcrow, J. A. K. Howard, *Dalton Trans.* **2004**, 1516–1518.
[26] C. J. O'Connor, *Prog. Inorg. Chem.* **1982**, *29*, 203–283.

[27] J. Pitarch López, F. W. Heinemann, R. Prakash, B. A. Hess, O. Horner, C. Jeandey, J.-L. Oddou, J.-M. Latour, A. Grohmann, *Chem. Eur. J.* **2002**, *8*, 5709–5722.
[28] J. Elhaïk, D. J. Evans, C. A. Kilner, M. A. Halcrow, *Dalton Trans.* **2005**, 1693–1700.
[29] E. Makovicky, T. Balić-Žunić, *Acta Crystallogr., Sect. B* **1998**, *54*, 766–773.
[30] P. Guionneau, M. Marchivie, G. Bravic, J.-F. Létard, D. Chasseau, *J. Mater. Chem.* **2002**, *12*, 2546–2551.
[31] D. F. Evans, *J. Chem. Soc.* **1959**, 2003–2005.
[32] E. M. Schubert, *J. Chem. Educ.* **1992**, *69*, 62.
[33] I. Weiss, H. Oberhammer, D. Viets, R. Mews, A. Waterfeld, *J. Mol. Struct.* **1991**, *248*, 407–414.
[34] J. McMurtrie, I. Dance, *Cryst. Eng. Commun.* **2005**, *7*, 216–229.
[35] P. Gütlich, H. A. Goodwin, D. N. Hendrickson, *Angew. Chem. Int. Ed. Engl.* **1994**, *33*, 425–427.
[36] G. Parkin, R. Hoffmann, *Angew. Chem. Int. Ed. Engl.* **1994**, *33*, 1462.
[37] J. A. Labinger, S. J. Weininger, *Angew. Chem. Int. Ed.* **2004**, *43*, 2612–2619.
[38] *COLLECT*, Bruker AXS Inc., **2002**, Madison WI, USA.
[39] *SHELXTL NT 6*.12, Bruker AXS Inc., **2002**, Madison WI, USA.
[40] T. Balić-Žunić, I. Vicković, *J. Appl. Crystallogr.* **1996**, *29*, 305–306.
[41] C. F. Macrae, P. R. Edgington, P. McCabe, E. Pidcock, G. P. Shields, R. Taylor, M. Towler, J. van de Streek, *J. Appl. Crystallogr.* **2006**, *39*, 453–457.

Received: February 6, 2009
Published Online: April 1, 2009

A typesetting error in the footnote of Table 2 has been corrected since the publication of this manuscript in the *European Journal of Inorganic Chemistry* Early View. The Editor.

